CLASP Promotes Microtubule Rescue by Recruiting Tubulin Dimers to the Microtubule

Bassam, Jawdat Al-; Kim, Hwajin; Brouhard, Gary; Oijen, Antoine van; Harrison, Stephen C.; Chang, Fred

Published in:
Developmental Cell

DOI:
10.1016/j.devcel.2010.07.016

Publication date:
2010

CLASP Promotes Microtubule Rescue by Recruiting Tubulin Dimers to the Microtubule

Supplementary Figures:

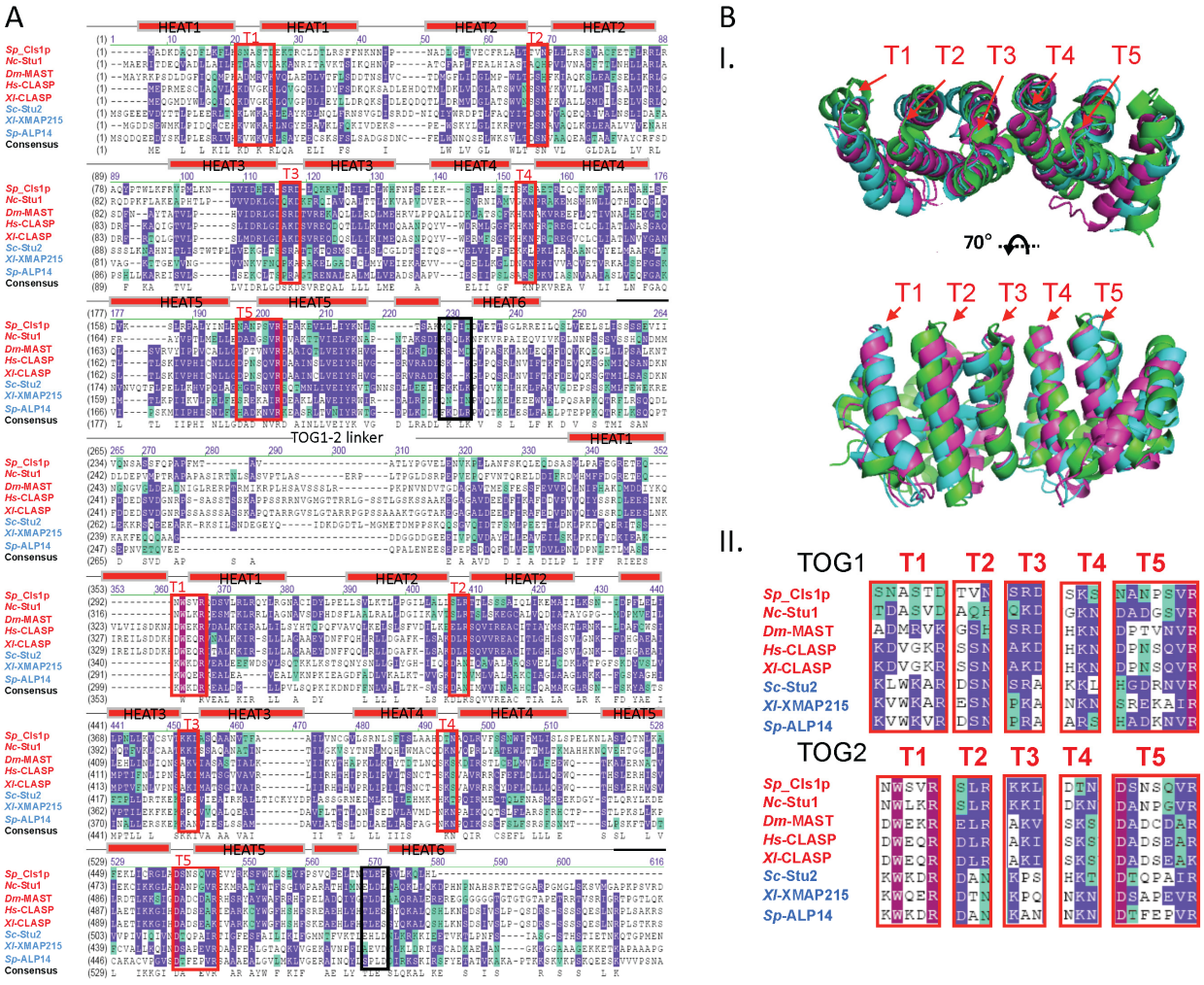

Figure S1: CLASP contains two conserved TOG-like domains and binds soluble αβ-tubulin dimer with defined stoichiometry and globular conformation

A) Sequence alignment of the CLASP and XMAP215/Dis1 family proteins reveals two conserved TOG domains in CLASP proteins. The N-terminal 500-600 residues of CLASP and XMAP215/Dis1 family proteins were aligned including sequences from *Schizosaccharomyces pombe* CLASP (Sp-Cls1), *Neurospora crassa* Stu1 (Nc-Stu1) *Drosophila melanogaster* MAST/orbit (Dm-MAST), human CLASP1 (Hs-CLASP1), *Xenopus Levi* CLASP1 (Xl-CLASP1), *Saccharomyces cereviaise* Stu2 (Sc-Stu2), *Xenopus laevis* XMAP215 (Xl-XMAP215), *Schizosaccharomyces pombe* ALP14 (Sp-ALP14). Domain boundaries were determined using the TOG structure alignment. Note conservation in intra-HEAT repeat turns (T1-T5, highlighted by red frames); CLASP TOG domains are likely to bind tubulin dimer.

B) Structural Superposition of XMAP215/Dis1 TOG domains Upper panel, structural features of XMAP215/Dis1 TOG domains: Two views (left, side view; right, top view) of aligned of structures of Stu2p TOG2 (cyan, PDB ID: 2QKI), Zyg9 TOG3 (green, PDB ID: 2OF3) and MiniSpindles TOG2 (purple, PDB ID: 2QK2), show the paddle-like structure of TOG domain composed of six conserved HEAT repeats; one narrow surface is lined by conserved intra-HEAT repeat turns (marked by red arrows). The alignment and figure were generated with the program Pymol. Lower panel: the isolated sequences of the five tubulin binding intra-HEAT repeat turns (T1 through T5) in TOG1 and TOG2 of CLASP proteins which were identified by structure-based sequence alignments in part A. The CLASP and XMAP215/Dis1 sequences are highlighted in red and blue, respectively.

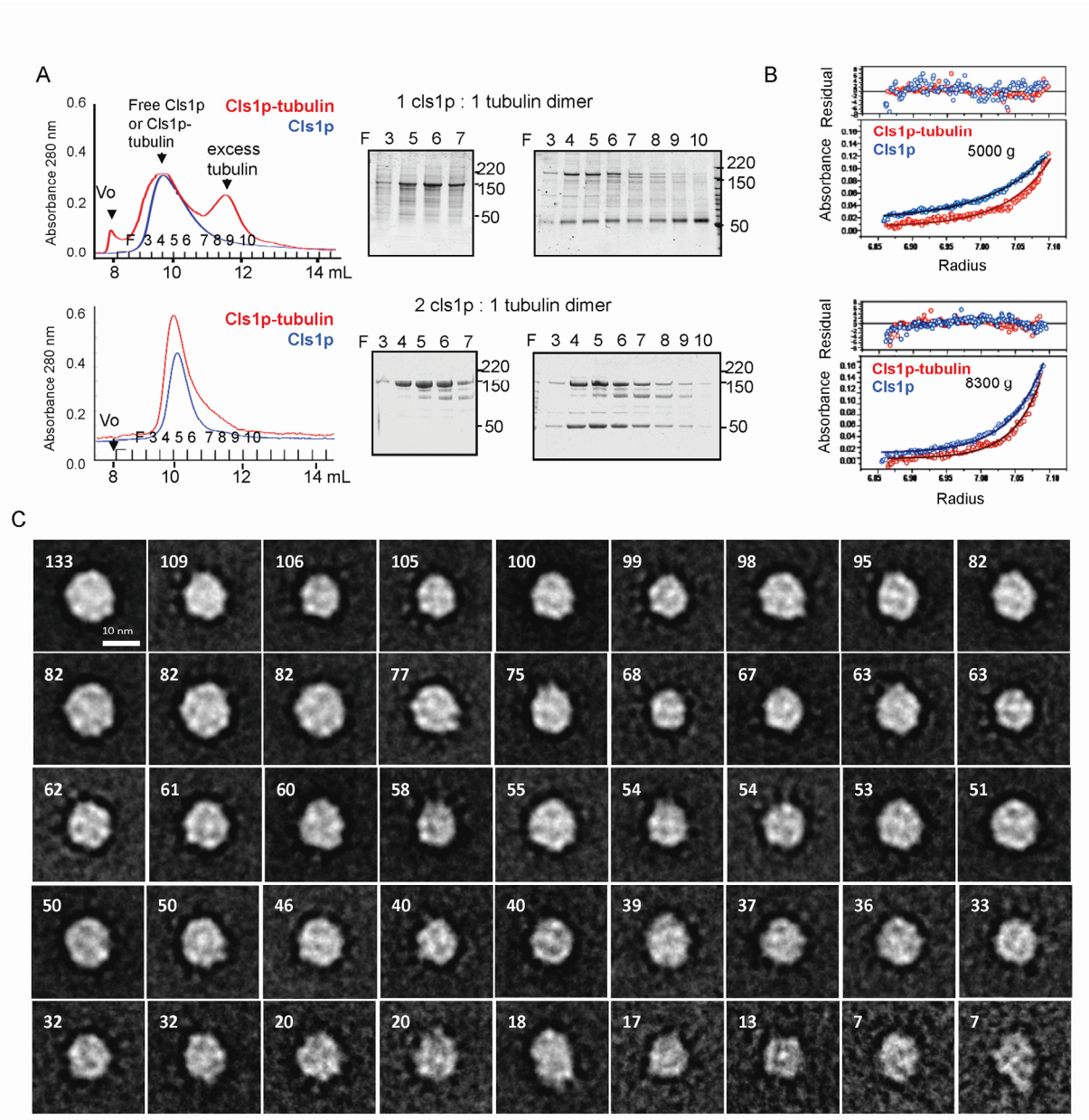

Figure S2: conformation and Stoichiomtry of Cls1-tubulin complex

A) Cls1p- tubulin complex Stoichiometry: ~ 2 mole Cls1p: 1 mole αβ-tubulin dimer. Varying the Cls1p amount to saturate a constant amount of soluble tubulin dimer into the Cls1p-tubulin complex peak on size exclusion chromatography indicates that 2 moles of Cls1p saturate by binding 1 mole of αβ-tubulin heterodimer. Asterisk (*) denotes a very small amount of degraded inactive Cls1p.

B) Sedimentation equilibrium analytical ultracentrifugation of Cls1p and purified Cls1-tubulin complexes at 5000 g and 8300 g. The lower panels show raw data (Cls1p: blue points, Cls1p-tubulin: red points) and calculated fit (Cls1p blue lines, Cls1p-tubulin: red lines) at the masses reported in table S1. The upper panels show the residual difference between actual data and the calculated fitted lines. Calculated and measured masses for Cls1p and Cls1p-tubulin complexes are shown in table S1.

C) Cls1p-tubulin complexes show defined globular organization. Forty five class average images of a reference free classification of 2700 Cls1p-tubulin negative stain EM images. The class averages are arranged in ascending order, with classes containing the highest number of images appearing first; the number of images averaged in each class is shown in white on each panel. We used a large number of classes in the classification to explore all possible conformational variation in Cls1p-tubulin images. The similarity of Cls1p-tubulin images among classes suggests that the number of classes we chose is higher than the variation in the EM images. We expect most of the variation to be due to deformations as a result of staining, if the particles adsorb to the grid in a preferential orientation, as appears to be the case.

Table S1: The detailed hydrodynamic and mass parameters for ClsIp constructs in the presence and absence of tubulin dimer measured by size exclusion chromatography or sedimentation equilibrium analytical ultracentrifugation

ClsI protein	Calculated Mass	Elution Volume	Stokes Radius	Apparent Weight	Measured Mass
αβ-tubulin (dimer)	101 kDa	14.01 mL	~41 Å	85 kDa	N/A*
ClsIp^{TOG} (monomer)	56 kDa	15.23 mL	~33 Å	40 kDa	45±5 kDa
ClsIp^{604} (monomer)	68 kDa	14.71 mL	~37 Å	65 kDa	60±5 kDa
ClsIp^{TOG}: tubulin	157 kDa	13.05 mL	~45 Å	120 kDa	N/A*
ClsIp^{604}:tubulin	171 kDa	12.54 mL	~51 Å	141 kDa	N/A*
ClsIp (dimer)	320 kDa	9.93 mL	~71 Å	517 kDa	†267±15 kDa
ClsIp : tubulin (2:1)	438 kDa	9.48 mL	~ 78 Å	675 kDa	†370±30 kDa
ClsIp-GFP- (dimer)	340 kDa	9.85 mL	~ 72 Å	530 kDa	†300±16 kDa
ClsIp-GFP:tubulin	460 kDa	9.30 mL	~ 79 Å	690 kDa	†400±15 kDa

***** These proteins or complexes were not stable enough for measuring mass by sedimentation equilibrium AUC

† The mass difference between ClsIp: tubulin and ClsIp is ~100 kDa, indicating a stoichiometry of 1 tubulin dimer per ClsIp dimer

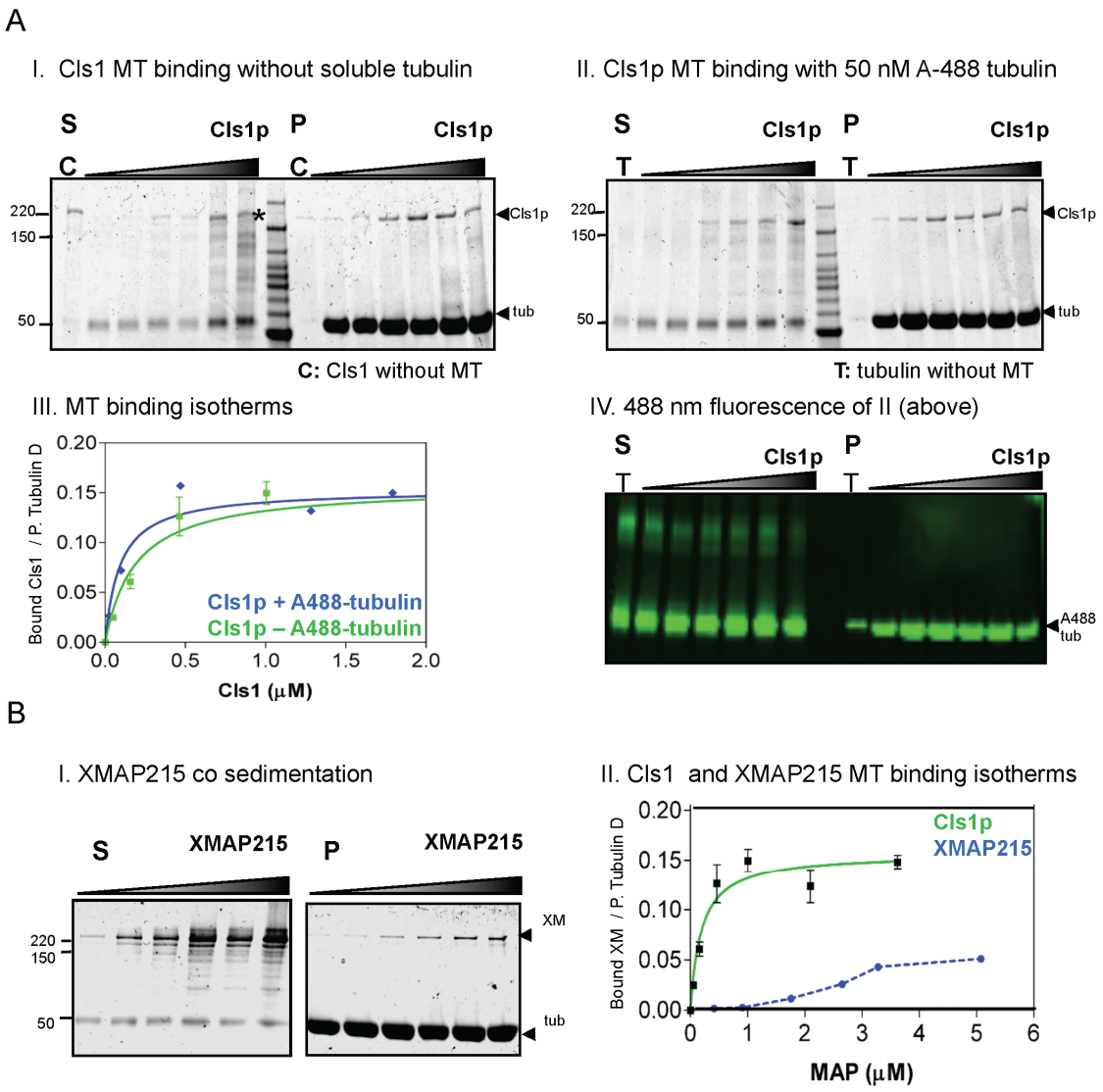

Figure S3: Cls1p binds MT lattices with high affinity S/R rich domain

A) **The presence of soluble tubulin dimer does not affect the high binding affinity of Cls1p to GMCPP-MTs.** Cls1 MT interaction recruits Alexa-Fluor-488 tubulin to MT lattices. Panel I and II, SDS-PAGE of supernatant (S) and pellet (P) of increasing concentrations of Cls1p added to a constant concentration of GMPCPP-MTs in the absence of Alexa-Fluor-488 tubulin dimer (panel I), and in the presence of tubulin dimer (upper Panel II). C and T, denote sedimentation experiments of Cls1p and AlexaF-488 tubulin alone the absence of GMPCPP-MTs, respectively. D: denotes proteolysis of Cls1p in supernatant lane. Panel III shows MT binding isotherms of Cls1p to GMPCPP-MTs in the presence of Alexa-488 tubulin (blue) and its absence (green). Y-axis is moles of Cls1p bound per moles of polymerized tubulin dimer. Panel IV, a 488 nm fluorescence scan of SDS-PAGE panel II showing AlexaF-488 tubulin co-sediments with MTs only in the presence of Cls1p.

B) MT co-sedimentation of XMAP215 on GMPCPP-MT. Panel I, SDS-PAGE of supernatant (S) and pellet (P) of increasing concentrations of XMAP215 added to a constant concentration of GMPCPP-MTs. Note that most of XMAP215 remains the supernatant suggesting weak affinity for MTs Panel II, MT binding isotherm of XMAP215 to MTs indicating a very weak binding, which does not saturate even at the highest concentrations. Y-axis indicates moles of Cls1p or XMAP215 per moles of polymerized tubulin.

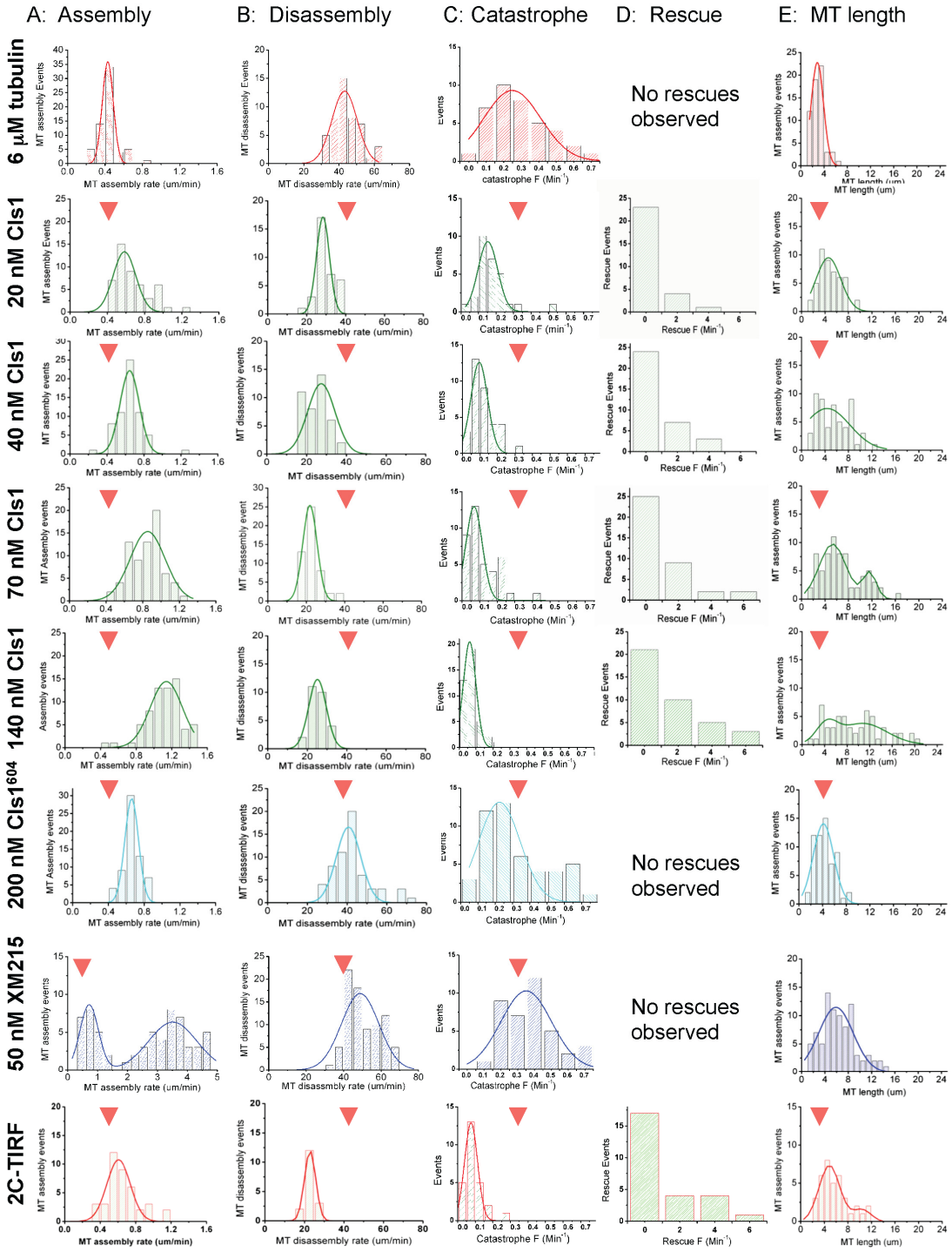

Figure S4: The Gaussian distributions of raw MT dynamic parameters

The distributions of MT dynamic parameter were measured from a large number of kymographs (shown in Fig 3A) for each dynamic TIRF experiment and the values were pooled for each experimental condition. The distributions of each parameter are plotted as the frequency of each event per number of observed events in each experiment. Distributions shown for the following conditions: 6 μM tubulin dimer alone (red curves), 6 μM tubulin + 50 nM XMAP215 (blue curves), 6 μM tubulin + 200 nM Cls1p^{604} (cyan curves), 6 μM tubulin + 20 nM Cls1p (green curves), 6 μM tubulin + 40 nM Cls1p (green curves), 6 μM tubulin + 70 nM Cls1p (green curves), 6 μM tubulin + 140 nM Cls1p (green curves) and 6 μM tubulin + 60 nM Cls1p + 10 mM Cls1p-GFP (labeled 2C-TIRF). Gaussians (lines in each curve) were used to fit the data and to estimate the average value of each parameter. Average values of each parameter are shown in Table S2. Red arrows mark the peak averages of MT dynamics parameters in 6 μM tubulin dimer to compare with other conditions.

Table S2: Parameters of dynamic microtubules measured by TIRF microscopy

Condition	N	Assembly		N	Disassembly		N	Catastrophe	N	Rescue	N	MT length
		Rate	total period		Rate	total period		Frequency		Frequency		
6 μM tubulin	63	0.43 ± 0.02	8.35 ± 0.69	47	43.4 ± 2.1	0.080 ± 0.011	49	0.30 ± 0.05		N / 0‡	60	2.1 ± 0.3
50 nM XMAP215	22	0.72 ± 0.1†	6.31 ± 0.55	82	49.0 ± 2.2	0.27 ± 0.035	41	0.40 ± 0.05		N / 0‡	85	5.9 ± 0.6
	41	3.51 ± 0.3†										
20 nM Cls1p	48	0.59 ± 0.05	10.54 ± 0.73	35	28.1 ± 1.1**	0.26 ± 0.022	28	0.13 ± 0.02**	28	0.64 ± 0.27	42	4.6 ± 0.7
40 nM Cls1p	62	0.65 ± 0.03*	13.28 ± 0.67	41	27.2 ± 2.1**	0.25 ± 0.034	40	0.10 ± 0.02**	40	1.14 ± 0.29*	57	4.4± 1.0
70 nM Cls1p	72	0.85 ± 0.05*	12.18 ± 0.75	50	22.4 ± 1.0**	0.19 ± 0.033	34	0.07 ± 0.02**	34	2.06 ± 0.53*	30	5.3 ±0.8 †
											39	11.6 ± 0.3 †
140 nM Cls1p	66	1.14 ± 0.05**	13.48 ± 0.57	27	25.4 ± 1.6**	0.20 ± 0.37	40	0.06 ± 0.01**	40	2.15 ± 0.40*	31	4.4 ± 0.7 †
											24	10.7 ± 1.7†
60 nM Cls1p+ 10 nM Cls1p-GFP	40	0.61 ± 0.04	12.89 ± 0.81	17	23.3 ± 1.4**	0.21 ± 0.032	26	0.08 ± 0.01**	25	1.49 ± 0.46*	30	4.8 ± 0.6†
											10	10.4 ± 0.9†
200 nM Cls1p^{TIT3}	90	0.70 ± 0.02	9.73 ± 0.75	71	29.3± 2.0**	0.23 ± 0.033	50	0.34 ± 0.04		N / 0‡	85	2.7 ± 0.3
200 nM Cls1p^{604}	63	0.66 ± 0.02	7.63 ± 0.48	59	41.2 ± 1.6	0.14 ± 0.013	48	0.23 ± 0.03		N / 0‡	60	4.1 ± 0.41

Units: Assembly rate (μm/min), Assembly period (min), Disassembly rate (μm/min) Disassembly period (min), Catastrophe Frequency (min^{-1}) Rescue Frequency (min^{-1}), MT length (μm)

Error reported is Standard Error Mean (SEM).

*Conditions significantly differ from 6 μM tubulin control at p> 0.01; Rescue frequencies were compared to 20 nM Cls1p.

** Conditions differ significantly from the 6 μM tubulin control at p> 0.001

For Assembly and disassembly rates, N is the number of assembly and disassembly events
For Catastrophe and Rescue frequency, N is the number of microtubules observed.
‡ Rescue events were not observed in these experiments
† these data showed a bimodal distribution and were fit with two Gaussian curves resulting into two different average rates.

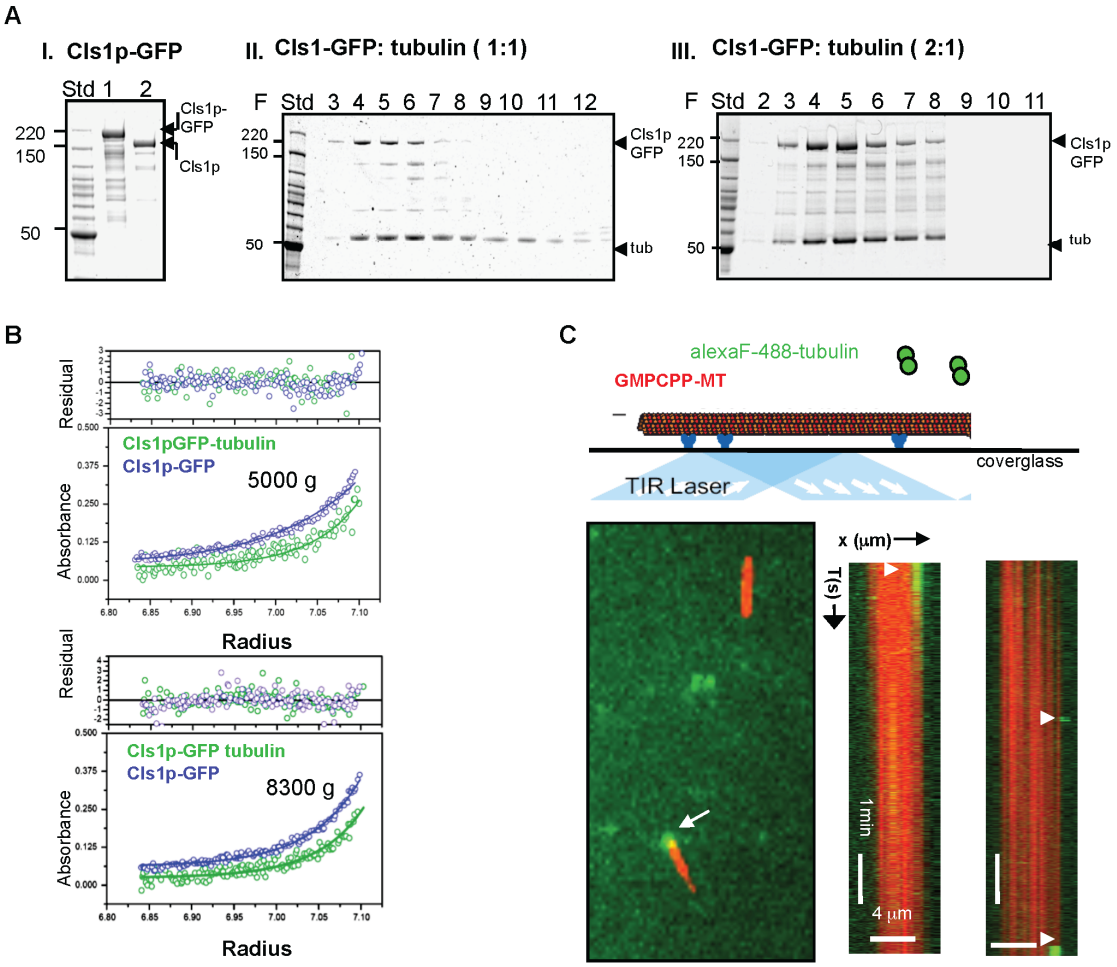

Figure S5: CLASP binds along GMPCPP-MTs without diffusion and recruit tubulin dimers

A) Clslp-GFP binds tubulin dimer at stoichiometry of 2:1 similar to untagged Clslp. Panel I, SDS-PAGE of purified Clslp and Clslp-GFP. Panel II, III: SDS-PAGE of Size exclusion chromatography experiment fractions of Clslp-GFP with tubulin dimer at 1:1 and 2:1 molar ratios, respectively.

B) Sedimentation equilibrium analytical ultracentrifugation of Clslp-GFP and purified Clslp-GFP-tubulin complexes at 5000 g and 8300 g. The fitted masses for Clslp-GFP and Clslp-GFP-tubulin complexes are reported in table SI. The lower panels show raw data (Clslp-GFP: blue points, Clslp-tubulin: green points) and calculated fit (Clslp blue lines, Clslp-tubulin: green lines). The upper panels show the residual difference between raw data and the calculated fitted lines. Calculated measured masses are shown in Table SI. Data in C, D show Clslp-GFP is a well-behaved dimeric protein that binds one tubulin dimer comparable to untagged Clslp.

C) Tubulin dimer does not bind the lattices of GMPCPP-MTs in the absence of Clslp. Top panel, schematic of TIRF experiment analyzing Alexa-Fluor-488 tubulin (green) association with Texas-red GMPCPP labeled MTs (red) in the absence of Clslp. Lower left panel, raw TIRF image of GMPCPP MTs and Alexa-Fluor-488 labeled tubulin dimer. Arrow denotes brief association of Alexa-488 tubulin with MT ends. Lower right panel, Kymographs showing very little association of Alexa-Flour-488 tubulin along the MT lattice except for brief binding at MT ends (arrowheads).

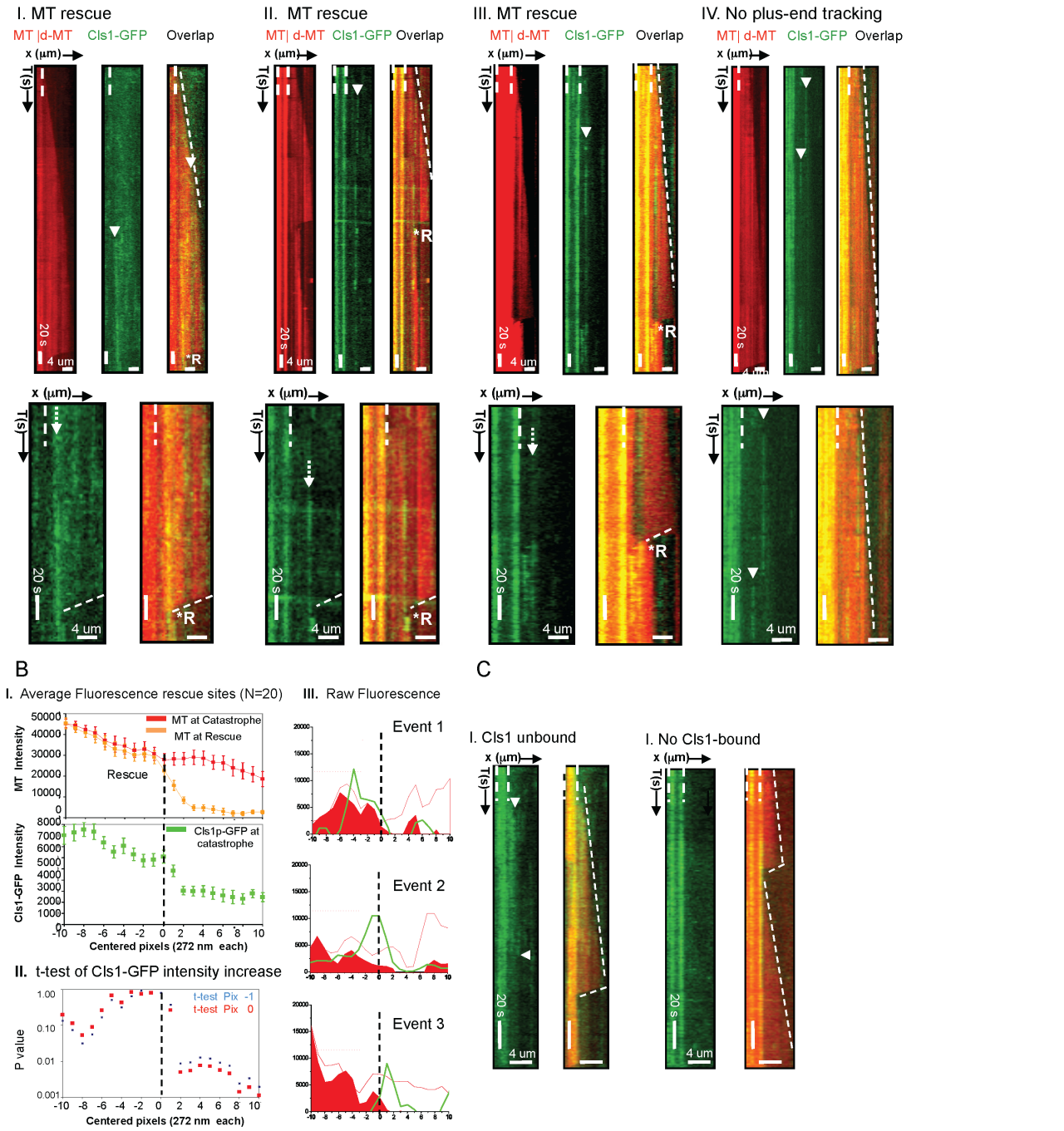

Figure S6: MT rescues are anticipated by sites with high Cls1p-GFP concentration along dynamic MTs

A) Additional examples of the correlation of MT rescue being anticipated by sites of high local Cls1p-GFP concentration, as shown in Fig 5C and D. Each panel shows a kymograph of dynamic MT (red), and Cls1p-GFP (green), an overlay of both, and higher magnification image in the lower panel. In Panels I-III, dynamic MTs assembly (white broken lines) followed by MT catastrophe and then MT rescue (R*) at high Cls1p-GFP concentration sites (arrowheads). Panel IV: Cls1p-GFP molecules bind densely along assembling MT and without tracking the MTplus end.

B) **Correlation of Cls1p-GFP intensity along a dynamic MT with the site of MT rescue.** Panel I shows an average fluorescence profile as seen in Figure 5E. Panel II, t-tests of Cls1p-GFP intensity at pixel -1 (blue) and pixel 0 (red) compared with the other pixel, show that Cls1-GFP intensity is significantly lower at sites upstream of site of rescue (pixels 2-10). Panel III shows the intensity profiles for three individual rescue events with Cls1p-GFP intensity (green), MT intensity at catastrophe (red lines) and at rescue (solid red). MT intensity is displayed at one-fifth the raw values.

C) Dynamic MTs do not show rescues when sites with high Cls1p-GFP concentration are not present. Panel I, kymograph of a dynamic MT and a single site with high Cls1p-GFP concentration formed (vertical arrow) and then dissociated (horizontal arrow). MT catastrophe is followed by disassembly to the MT-seed without rescue. Panel II, a kymograph of dynamic MT where high concentration of Cls1p-GFP did not form. MT catastrophe disassembled the dynamic MT to the seed. Note that a high Cls1p-GFP concentration is bound along MT seeds throughout.

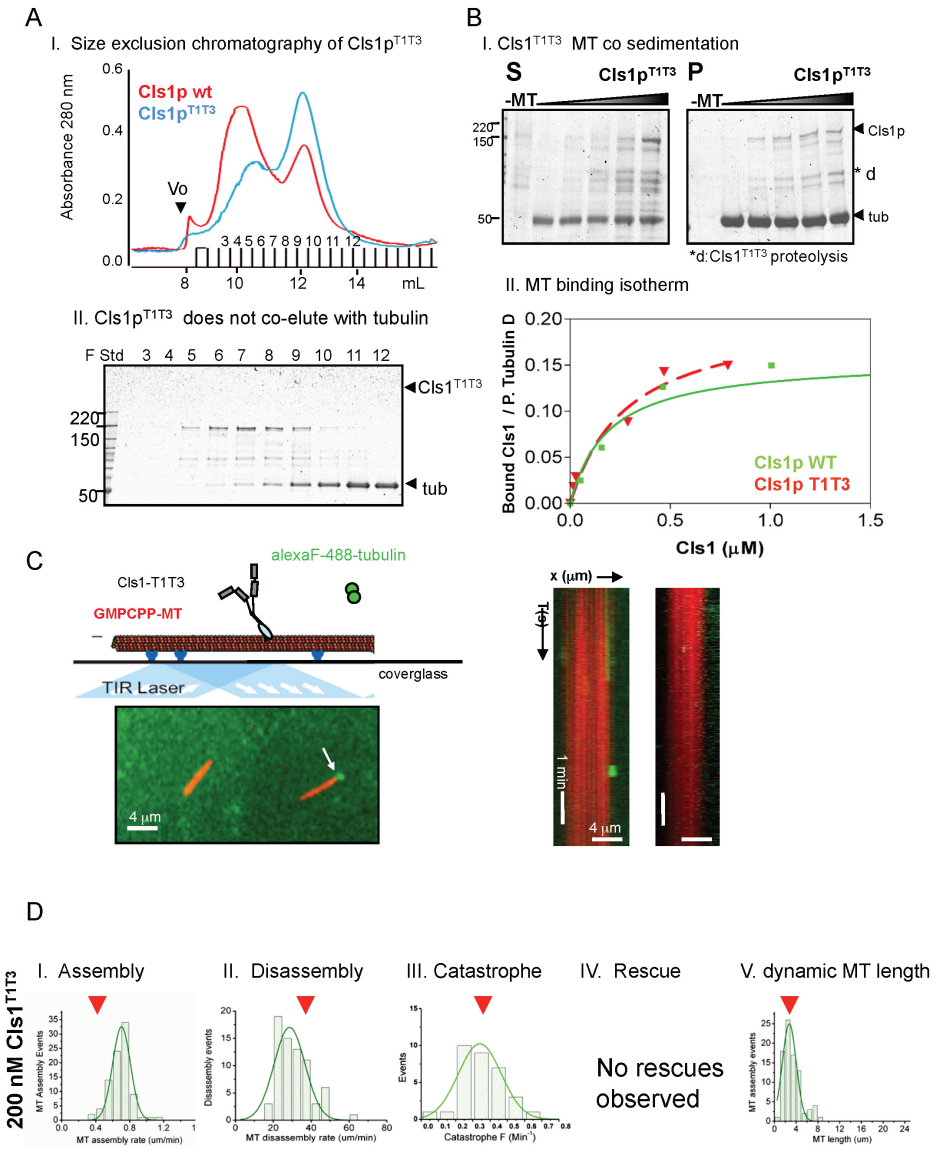

Figure S6: Biochemical properties of TOG defective mutant Clslp (Clslp^{T1T3})

A) **Clslp^{T1T3} does not form a complex with the tubulin dimer,** Panel I, Size exclusion chromatography of Clslp^{T1T3} mixed with tubulin (blue) compared with wild type Clslp mixed with tubulin (red) shown in Fig 6A and Fig 2A. Panel II, SDS-PAGE of fractions Clslp^{T1T3} and tubulin, note that the two proteins do not co-elute.

B) **Clslp^{T1T3} binds to GMCPP MTs with high affinity** MT co-sedimentation of Clslp^{T1T3} on GMPCPP-MT. Panel I, SDS-PAGE of supernatant (S) and pellet (P) of increasing concentrations of Clslp^{T1T3} added to a constant concentration of GMPCPP-MTs. Note that most of Clslp^{T1T3} co sediments at the low concentrations and saturates at higher concentrations suggesting high affinity for MTs. Panel II, MT binding isotherm of Clslp^{T1T3} (red) and Clslp wt (green, Figure 2E) to GMCPP-MTs indicate similar binding affinities and saturation stoichiometries. Y-axis is the moles of Clslp bound to moles of polymerized tubulin dimer. d: denotes some proteolysis of Clslp^{T1T3}

C) Clslp^{T1T3} does not recruit tubulin dimer to GMCPP MT lattices Top panel, scheme of TIRF experiment of 50 nM Clslp^{T1T3} to recruiting 50 nM alexaF-488 tubulin (green) to Texas-red GMPCPP labeled MTs (red). Lower panel, raw image of GMPCPP MTs (red) and AlexaF-488 labeled tubulin dimer (green). Arrow denotes brief association of Alexa-488 tubulin with MT ends. Lower right panel, Kymographs showing no recruitment of AlexaF-488 tubulin by Clslp^{T1T3} along the MT lattice except for brief binding at MT ends, similar to Figure S4C.

D) Clslp^{T1T3} does not decrease MT catastrophes nor activate MT rescues The effect of Clslp^{T1T3} mutant on the distributions of dynamic MT parameters (assembly rate, disassembly rate, catastrophe frequency and rescue frequency) by determined by TIRF microscopy as described above for Clslp in Fig 3 and Fig S4. Values of the average parameters from the Gaussian fits of these distributions are in Table S2.

Table S3: The detailed statistics of TOG mutant Cls1p defects in rescuing Cls1p function at low expression (with thiamine), and defects in MT stabilization at high expression conditions (without thiamine), as described in Fig 6.

Cls1 Mutant	TOG2 Mutation	Nat-resistant colonies (%)	Std. Dev	No. of cells	Cells stabilized MTs (%)	No. of cells
Cls1T1T3T5	W293A K379A K380A R465A	2.06	0.84	1516	1.06	94
Cls1T1T3	K379A K380A R465A	2.64	1.81	1354	2.17	138
Cls1T1T5	W293A R465A	6.43	0.47	802	0.00	110
Cls1T5	R465A	19.62	4.06	462	31.43	70
Cls1T1T3	W293A K379A K380A	2.51	2.19	2052	0.00	149
Cls1T3	K379A K380A	1.36	1.74	1120	0.72	138
Cls1T1	W293A	3.92	2.21	966	4.55	110
Vector control	Vector control	1.37	0.33	6878	1.79	56
Cls1 wild type	Wild type cls1+	47.85	3.45	886	78.26	69

Supplementary Materials and Methods

S. pombe Clr1p constructs, protein expression and purification

Constructs of full-length *S. pombe* Clr1p, Clr1p^{TIT3} (residues 1-1462 with or without C-terminal GFP), Clr1p^{TOG} (residues 1-500) and Clr1p^{604} (residues 1-604) were cloned by ligation-independent cloning (LIC) into a modified baculovirus expression vector, in frame with an N-terminal his-maltose binding protein tag (MBP) flanked by a TEV protease cleavage site to improve protein expression and solubility. Protein expression was carried out by infecting 2 L of Hi5 insect cells at a density of 1X10^{6} cells/mL with the amplified baculoviruses. After 60-72 h, insect cells were harvested and resuspended in lysis buffer (50 mM HEPES, 250 mM KCl, 10 mM imidazole, pH 7.0) and lysed with a dounce homogenizer. Lysates were clarified by centrifugation at 60000 x g for 40 min. His-MBP-tagged fusion proteins were isolated by metal affinity chromatography (NTA-agarose, Quiagen) and eluted using a 10-400 mM imidazole linear gradient in lysis buffer. N-terminal His-MBP tags were cleaved, overnight, with 5 U/ml TEV protease and 1 mM dithiothreitol. Clr1p or Clr1p^{TIT3} constructs (with or without a C-terminal GFP) were dialyzed against binding buffer (50 mM HEPES 100 mM KCl, 5 mM D-mercaptoethanol, pH 7.0), loaded onto a MonoQ anion exchange column, and eluted using a gradient of 100-700 mM KCl. Clr1p containing fractions were concentrated and loaded onto a Superdex 200 gel filtration column (16/60) equilibrated with binding buffer containing 300 mM KCl and eluted in 1 ml fractions. The Clr1p^{604} and Clr1p^{TOG} constructs were purified using MonoS ion exchange chromatography followed by gel filtration chromatography as described for the Clr1p constructs.

Biophysical analyses of Clr1p, Clr1p^{TOG}and Clr1p^{604} and their complex with tubulin dimer

Size exclusion chromatography (SEC), Clr1p and Clr1p^{TOG} constructs were allowed to form complexes with various amounts of tubulin dimer for 5 minutes, and were loaded onto a 10/5 Superdex 200 column pre-equilibrated at 4°C with 25 mM HEPES, 80 mM KCl, 1 mM EGTA, pH 7.0, and eluted in 0.5 ml fractions. Fractions were evaluated by SDS-PAGE. Apparent molecular masses and Stokes radii of the Clr1p constructs alone and in complex with tubulin dimer were determined by calibrating the size-exclusion column with protein standards (Biorad Inc.). Stokes radii for different samples were calculated as averages of the Porath and Laurent-Killander Stokes' radii, which matched closely. For sedimentation equilibrium analytical ultracentrifugation experiments, purified fractions of Clr1p and Clr1p^{TOG} and Clr1p^{604} with and without tubulin were loaded in an Optima XLA Beckman Coulter analytical ultracentrifuge as previously described (Al-Bassam et al, 2006).

Electron microscopy and classification of Clr1p-tubulin complexes

A total of 2700 Clr1p-tubulin particle images were selected with the program Ximdisp (Smith, 1999). Images of single Clr1p-tubulin particles were aligned into 45 different classes using reference-free hierarchal ascendant classification in the program SPIDER (Shaikh et al, 2008). Multiple rounds of shift and rotation parameter refinement were carried out to improve the alignment of single images in each of the class averages. The observed similarity among many classes strongly suggests that the number of classes is higher than the degree of diversity in the particle images (Fig S2C).

Total internal reflection microscopy: surface treatment and imaging conditions

TIRF flow cells were treated with following solutions: 1) 0.03 mg/ml anti-biotin monoclonal antibody (invitrogen) diluted in flow buffer (80 mM PIPES, 80 mM KCl, 4 mM $MgCl_2$, 1 mM EGTA, pH 6.8), and then washed twice in flow buffer. 2) 1% Pluornic-F127 in flow buffer to neutralize the remaining surface and then washed extensively with flow buffer. 3) 0.1 mg/ml GMPCPP stabilized MT seeds. The TIRF flow cell was then equilibrated with imaging buffer (flow buffer + 1 mM GTP + photo-bleaching protection cocktail: 0.1 % D-mercaptoethanol, 0.4% glucose, 20 µg/ml catalase (Roche), 20 µg/ml glucose oxidase (sigma-Aldrich)). TIRF imaging was carried out in flow cells that were warmed by a contact Nikon TIRF objective using a collar heater set to 35 °C. MT dynamics were observed by an evanescent wave generated from the total internal reflection of 488 and 568 nm filtered-laser light generated from an Argonne laser. For each data set, 1000 consecutive (2.1 s intervals) images were collected on a side entry dual-split iXon EM CCD (Andor Sciences).

TRIF microscopy of dynamic or static MTs in the presence or absence of Cls1p

For MT dynamics measurements (diagramed in Fig 3A), 5.4 µM unlabeled tubulin dimer and 0.6 µM Alexa-Fluor-488 labeled tubulin dimer were diluted in imaging buffer (80 mM PIPES, 80 mM KCl, 4 mM $MgCl_2$, 1 mM EGTA, pH 6.8, 1 mM GTP photo bleaching protection cocktail (see supplementary method)) in the absence or the presence of Cls1p or XMAP215. Flow cells were equilibrated with imaging buffer and were imaged as described above. To image Cls1p-GFP localization (diagramed in Fig 4A), 10 nM or 50 nM Cls1p-GFP were added to imaging buffer (containing no GTP), and then equilibrated into a flow cells with attached Texas-Red GMPCPP MT seeds. To image Alexa-Fluor-488 labeled tubulin recruitment by Cls1p or $Cls1^{TIT3}$ (diagramed in Fig 4B), 5 nM Alexa-Fluor-488 labeled tubulin was mixed with 45 nM unlabelled tubulin and added to 50 nM Cls1p, 50 nM $Cls1p^{TIT3}$ or their absence in imaging buffer (containing no GTP). TIRF images were collected as described above.

Dual Color TIRF imaging Cls1p-GFP and dynamic MTs.

Dual-color TIRF imaging of Cls1p-GFP and dynamic MTs (Fig 5A) was carried out as follows. Texas red labeled GMPCPP MT seeds were attached to the surface as described above, 5.8 µM unlabeled tubulin and 0.20 µM Texas-red labeled tubulin were mixed with 60 nM FL-Cls1p and 10 nM Cls1p-GFP. Flow cells were equilibrated with the above mixture in imaging solution, and TIRF imaging was carried out as described above.

Image analysis of dynamic MTs and Measurement of dynamic MT parameters

Kymographs were constructed for dynamic MTs growing from each MT seed using the EMBL ImageJ software package, to study the transitions and rates of assembly and disassembly. MT assembly and disassembly rates were measured as slopes in kymographs of individual dynamic MTs. Frequencies of MT catastrophe and MT rescue events were measured for individual dynamic MTs formed from each MT seed by dividing the number of events with the duration of MT assembly (for catastrophe) and MT disassembly (for rescue). A rescue event was identified by a reversal of measureable disassembly (at least 10 pixels) back to assembly. MT pauses were extremely rare and were not counted as rescue events. The distributions for assembly rates, disassembly rates, catastrophe frequency, and rescue frequencies were binned into histograms and then fit by single or multiple Gaussian functions to determine the average and error values for each parameter using the program Origin (Originlab). Fluorescence intensity profile scans of Cls1p-GFP along dynamic MTs were performed by

averaging pixel intensity across three successive frames and plotting the intensity distribution to identify peaks corresponding to sites of high Clsp1-GFP density and are shown (Fig S6B). Average fluorescence intensity profiles of Clsp1-GFP at the sites of rescue (Fig 5E, Fig S6B) were calculated as follows: intensity profiles for the MT at catastrophe, MT at rescue, and Clsp1-GFP were calculated for individual rescue events and background intensity for each was subtracted. Pixel numbers for individual events were shifted so the rescue site are centered at 0 positions and then intensity profiles for MT intensities at catastrophe, MT intensities at rescue and Clsp1-GFP intensities at catastrophe were independently averaged for 20 events (Fig 5E). The significance of Clsp1-GFP intensity increase at sites of rescue (pixel 0, -1) compared to other sites was calculated using student t-tests and the Cls1-GFP increase at the rescue site was increase significantly than any site prior (Fig 5E, Fig S6B, II).

Single particle tracking and simulations of Clsp1 binding to MTs

Tracking of Clsp1-GFP puncta was performed in the software package Kalaimoscope (Transinsight GmbH). The diffusion coefficient for Clsp1 was calculated as previously described (Helenius et al., 2006). Trajectories for Clsp1-GFP puncta were exported from Motion Tracking to MATLAB (The MathWorks) for further analysis. Curve fitting was performed in OriginPro (OriginLab).

A simulation of Clsp1 binding to MTs, based on the concept of "model-convolution" (Gardner and Odde, 2010), was programmed in MATLAB (The MathWorks). In brief, Clsp1 molecules were distributed to locations on the MT lattice (see below). The molecules were assigned intensity, convolved with an experimentally measured point-spread-function. A pixel-grid was super-imposed to create an artificial image and noise was added. The modeled distribution of Clsp1 binding was either random (figure 4F, #1) or based on a physical model of clustering (Figure 4F,# 2-4) in which incoming Clsp1 molecules "scan" a region of the MT adjacent to their initial location in an attempt to form a cluster. The range of this "scan" can be varied, but is ultimately derived from the diffusion coefficient and lifetime of a Clsp1 interaction. The artificial images generated by this simulation were qualitatively compared to images of Clsp1-GFP binding to MTs.

References

Al-Bassam, J., van Breugel, M., Harrison, S. C., and Hyman, A. (2006). Stu2p binds tubulin and undergoes an open-to-closed conformational change. J Cell Biol *172*, 1009-1022.

Helenius, J., Brouhard, G., Kalaidzidis, Y., Diez, S., and Howard, J. (2006). The depolymerizing kinesin MCAK uses lattice diffusion to rapidly target microtubule ends. Nature *441*, 115-119.

Gardner, M. K., and Odde, D. J. Stochastic simulation and graphic visualization of mitotic processes. Methods *2010*, 22.

Shaikh, T. R., Gao, H., Baxter, W. T., Asturias, F. J., Boisset, N., Leith, A., and Frank, J. (2008). SPIDER image processing for single-particle reconstruction of biological macromolecules from electron micrographs. Nat Protoc *3*, 1941-1974.

Smith, J. M. (1999). Ximdisp--A visualization tool to aid structure determination from electron microscope images. J Struct Biol *125*, 223-228.